ACS APPLIED MATERIALS & INTERFACES

Research Article

www.acsami.org

High-Performance Nanoporous TiO_2/La_2O_3 Hybrid Photoanode for Dye-Sensitized Solar Cells

Hua Yu, Bofei Xue, Porun Liu, Jingxia Qiu, William Wen, Shanqing Zhang,* and Huijun Zhao

Centre for Clean Environment and Energy, Environmental Futures Centre and Griffith School of Environment Gold Coast Campus, Griffith University, QLD 4222, Australia

ABSTRACT: An organic lanthanum solution was prepared and used for modifying the nanoporous TiO_2 photoanode for dye-sensitized solar cells (DSSCs). The preliminary characterization results demonstrate that La_2O_3 was formed on the surface of the TiO_2 photoanodes. The X-ray diffraction (XRD) and X-ray photoelectron spectroscopy (XPS) analyses suggest that La^{3+} was introduced into the TiO_2 nanocrystalline, while, the scanning electron microscopy (SEM) and tunnelling electron microscopy (TEM) characterizations suggest that a thin La_2O_3 layer forms on surface of the TiO_2 nanostructure. The La_2O_3 layer is able to alleviate the electron recombination as a passivation layer. Though the slight decrease in surface areas were induced by the surface modification, the dye loading were maintained, which can be attributed to the formation of strong co-ordination bonding between the dye molecules and the lanthanide. The bonding can also facilitate the electron transfer between the dye molecules and TiO_2 conduction band. Consequently, the open circuit potential and short circuit current were boosted significantly and the overall energy conversion efficiency of the DSSCs was remarkably improved from 6.84% for the control film to 9.67% for the La^{3+}-modified film.

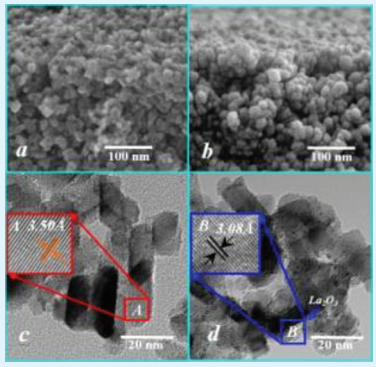

KEYWORDS: *TiO_2/La_2O_3 photoanode, DSSCs, dye adsorption, electron transportation*

1. INTRODUCTION

Dye-sensitized solar cells (DSSCs) have been considered as a low-cost and efficient solar-to-electricity conversion device.[1,2] To date, nanoporous TiO_2 are still the most promising materials for DSSCs photoanodes.[3] The nanoporous nature of the TiO_2 nanomaterials provides high surface area for efficient dye adsorption, which imparts high light harvesting and energy conversion efficiency.[4] However, electron recombination in the electron transport processes, including the electron injection from the excited dye to the TiO_2 conduction band and electron transport from the conduction band to the conductive substrate, is considered as one of the major obstacles to achieve high solar-to-electricity conversion efficiency.[5]

Tremendous efforts have been devoted to modify the nanoporous TiO_2 photoanodes for alleviating the electron recombination.[2] TiO_2 surface modification with an insulating layer, such as $BaCO_3$,[6] Al_2O_3,[7] and MgO,[8] or a higher conduction band edge semiconductor layer, such as ZrO_2,[9] In_2O_3,[10] Nb_2O_5,[11] and ZnO,[12] was proven effective in reducing the recombination and increasing the DSSCs conversion efficiency.[12] However, deposition of an additional surface layer could interfere the dye loading and the electron injection processes, which could affect the energy conversion efficiency, leading to limited improvement in energy conversion efficiency.[9]

Lanthanide ions are known for their ability to form complexes resulted from the co-ordination bonding between the *f* orbitals of the lanthanides and lone electron pairs of various Lewis bases (e.g., acids, amines, aldehydes, alcohols, thiols, etc.) because of the abundant functional groups.[13] Among the lanthanide ions, La^{3+} was successfully incorporated into a TiO_2 structure for improving the adsorption of the organic compounds rate.[13,14]

Recently, we used an organic TiO_2 solution to modify the nanoporous TiO_2 photoanodes to construct a compact thin layer on the surface of the nanoporous TiO_2 networks.[15] The dip coating method is efficient, simple and low-cost in surface modification. It is believed that the organic property of the solution is crucial for obtaining this compact thin layer.[15]

Based on the aforementioned findings, we propose to introduce a compact thin La_2O_3 layer on the surface of the nanoporous TiO_2 networks using an organic lanthanum solution in this work. Considering the low viscosity nature of the organic lanthanum solution, we expect the La^{3+} can be introduced throughout the photoanode, enhancing dye adsorption strength and improving electron transport efficiency, and thus boost the performance of the resultant DSSCs.

2. EXPERIMENTAL SECTION

2.1. Materials. Lanthanum nitrate hexahydrate (>99.9%), chloroplatinic acid hydrate (≥ 37.50% Pt basis), and isopropanol (>99.7%) were purchased from Sigma-Aldrich. TiO_2 paste, N719 dye ($RuL_2(NCS)_2(TBA)_2\cdot(H_2O)_4$, L = 2,2′-bipyridyl-4,4′-dicarboxylic acid, TBA =tetrabutylammonium) and organic based liquid electrolyte (HPE, Dyesol) containing I^-/I_3^- redox couple were supplied by Dyesol (Australia), compositing of gamma butyrolactone, iodine, lithium iodide

Received: November 8, 2011
Accepted: February 10, 2012
Published: February 10, 2012

and imidazole compound. Fluorine-doped tin oxide (FTO) transparent conductive glass (≤14 ohm/square) from Pilkington was used as the substrate.

2.2. TiO_2 Films Preparation and Modification by Organic Lanthanum Solution. TiO_2 films were screen-printed on precleaned FTO glass with commercial TiO_2 paste. The printing processes were repeated until a thickness of 12 μm was obtained. Subsequently the resultant films were sintered at 450°C for 30 min, designated as control films. The organic lanthanum solution as a modification precursor was prepared by dissolving 2.165 g $La(NO_3)_3 \cdot 6H_2O$ into 100 mL of isopropanol under vigorous stirring for 20 mins. Modification of the control films was achieved by using a dip-coating technique with a withdrawing speed of 2 mm/s from the lanthanum solution, dried in air and subsequently sintered at 450 °C for 30 min. The modified films with coating layers of 1, 2, 4, 6, 8, and 10 are marked as M1, M2, M4, M6, M8, and M10, respectively.

2.3. Characterizations of TiO_2 Films. The materials characterizations were carried out by X-ray diffraction (XRD, Philips PW3020), X-ray photoelectron spectroscopy (XPS, Physical Electronics 549), scanning electron microscopy (SEM, JEOL 890), transmission electron microscopy (TEM, JEOL 4010), The XPS survey was conducted using the position of the C 1s peak (284.6 eV) of adventitious carbon as charge referencing UV−vis diffuse reflectance spectroscopy and UV-vis spectrophotometry (Varian, Cary 4500).

2.4. DSSC Assembly and Characterizations. The control films and modified films with a sensitized area of 1 cm^2 were immersed into N719 dye solution (3×10^{-4} M in butanol and acetonitrile, 1:1, v/v) for 24 h. The dye-sensitized films were washed with anhydrous acetonitrile after dye sensitization, and dried in N_2 flow before the DSSC fabrication.[15] Platinum counter electrode on FTO substrate was prepared by spin-coating using 5 mM H_2PtCl_6 isopropanol solution and pyrolyzing the resulting film at 380 °C for 15 min.[15] Liquid solution containing I^-/I_3^- redox couple was used as the supporting electrolyte. Then the dye-sensitized TiO_2 film, electrolyte and platinum counter electrode were configured into a typical sandwich cell and sealed with a thermoplastic sealant. A mask with a window area of 0.15 cm^2 was used to define the active illumination area of the DSSCs.

The photovoltaic measurement of the DSSCs was conducted using a Scanning Potentiostat (PAR362, Princeton) under 100 mW cm^{-2} illumination via a 500W Xe lamp (*Trusttech*, Beijing, China) coupled with an AM 1.5G filter (Sciencetech, Canada). The light intensity was measured by a radiant power meter (Newport 70260, USA) equipped with a broadband probe (Newport 70268, USA). The measured photovoltaic parameters including short-circuit photocurrent (J_{sc}), open-circuit photovoltage (V_{oc}), fill factor (FF) and energy conversion efficiency (η) were the average value of four cells and the corresponding statistical errors were 3%, 3%, 2% and 3%, respectively. Open circuit voltage decay (OCVD) experiment was conducted by monitoring the subsequent decay of V_{oc} after cutting off the illumination on DSSCs under open-circuit condition.

3. RESULTS AND DISCUSSION

3.1. Materials Characterizations. The organic lanthanum solution allows the La^{3+} ions to readily penetrate the entire nanoporous TiO_2 framework and enables the establishment of a thin and uniform layer coating on the nanoporous TiO_2 surface. The post-thermal treatment converts the thin coating layer into the highly crystalline La_2O_3 film. The thickness of the coating layer with optimized coating times is expected not to significantly change the porosity of the original nanoporous structure (affecting the dye adsorption capacity and optical property), and more importantly, to play an important part for efficient electron transport.[9] The sample M8 is used as a typical example of the modified films in the following discussion if not otherwise stated.

The crystalline structure and element analysis of control and modified films were analysed by the XRD spectra as shown in Figure 1. Typical anatase (A) peaks at 2θ of 25 and 37°[16] were

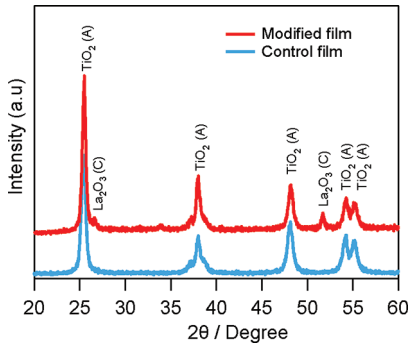

Figure 1. XRD patterns of the control and M8 modified films; TiO_2 (A), anatase; La_2O_3 (C), cubic La_2O_3 phase.

observed in the spectra of both the control and modified films. For the modified photoanodes, two diffraction peaks at about 2θ of 27 and 52° (JCPDS; 22-369)[17] indicate the presence of cubic(C) La_2O_3 phase.

Further elementary investigation of the films was conducted by the XPS spectra (Figure 2). The binding energy for this

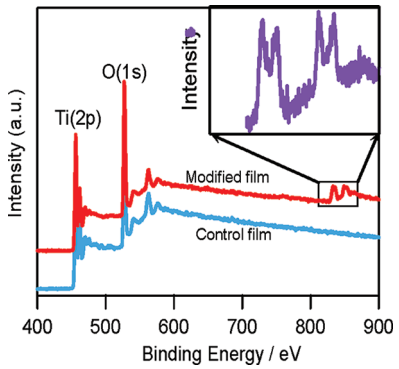

Figure 2. XPS survey of the control film (blue curves) and M8 modified film (red curves). The insert is the magnified spectrum in the range of 510−870 eV.

measurement was calibrated by using the C(1s) line (284.6 ± 0.1 eV) from adventitious carbon. The survey spectrum of the control film in Figure 2 show that there are no binding peaks for the control film when the binding energy is greater than 600 eV. In contrast, for the modified film, the binding energy peaks were observed at 834.8 ± 0.1 eV, 840.4 ± 0.1 eV, 851.8 ± 0.1 eV, and 856.4± 0.1 eV. These responses are correspondent to the 3d states of the La element (see the high-resolution spectrum in the insert of Figure 2), respectively.[18] Interestingly, the effect of the La^{3+} on the valence state of the TiO_2 crystallite can be observed by the XPS study. Figure 2 shows the binding energy peaks of Ti (2p) of the control and modified films.

Figure 3 shows the SEM and TEM images of the control and modified films. The SEM image in Figure 3a exhibits a typical nanoporous structure, where TiO_2 nanoparticles are randomly packed across the entire layer, forming pores and gaps among TiO_2 particles. Most TiO_2 particles were in regular cuboid shapes with particle sizes ranging from 20 to 30 nm as confirmed by the TEM image in Figure 3c. In contrast with the control film, the SEM image of the modified film in Figure 3b reveals a more densely packed nanoporous structure. The overall surface roughness seems similar to those observed from the control film, but the number of large pores and gaps is found to be reduced.

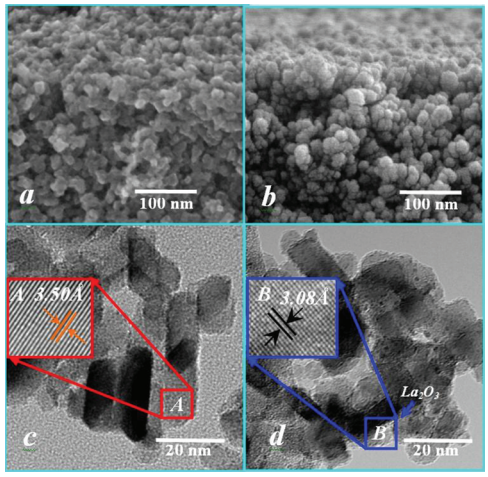

Figure 3. Cross-sectional SEM images of (a) the control film and (b) M8 modified film; TEM images of (c) the control film and (d) M8 modified film.

It also can be seen that the edges of the original cuboid particles were smoothened. This is apparently resulted from the coating of the La_2O_3 film, which could be further confirmed by the TEM analysis as shown in images c and d in Figure 3. Figure 3c shows the TiO_2 nanoparticles in the control samples have a sharp edge. In strong contrast with this, Figure 3d shows that the TiO_2 nanoparticles in the modified sample are not as sharp as the ones in control sample. As a matter of fact, a thin layer can be observed on the surface of the TiO_2 nanoparticles. The lattice fringe spacing of the control and modified samples were calculated using the high resolution results. The lattice fringe spacing of the TiO_2 particles for the control sample is 3.52 Å corresponding to the (101) facet of anatase TiO_2 (see Figure 3c),[19] whereas the lattice fringe spacing of the coating particles in the modified sample is 3.05 Å, which is corresponding to the (011) face of La_2O_3 (see Figure 3d).[20]

The average thickness of the La_2O_3 layer can be estimated from the correspondent TEM images and are listed in Table 1.

Table 1. Average La_2O_3 Thickness (d) Estimated by the TEM Method, the Surface Area (s) Measured by the BET Method, the Electron Transfer Resistance (R_0) Measured by the Photoelectrochemical Method and Dye Adsorption Amount (Ads.) Measured by the NaOH Ethanolic Solution Desorption Method for the Control and Modified Films

electrodes	d (nm)	s (m^2/g)	R_0 (Ω)	Ads. (mol/cm^2)
control film		61.50	399	1.67×10^{-7}
modified film (M1)	3	59.69	407	1.72×10^{-7}
modified film (M2)	5	57.22	398	1.69×10^{-7}
modified film (M4)	6	56.93	371	1.66×10^{-7}
modified film (M6)	7	56.17	304	1.63×10^{-7}
modified film (M8)	8	55.81	261	1.64×10^{-7}
modified film (M10)	10	53.20	456	1.57×10^{-7}

There is a clear trend that the average thickness increases with the increase of the coating times. The actual thickness of the La_2O_3 coating layer also depends on the geometry and TiO_2 particles and the location of the joining points. For the M8 sample, it is normally thicker at the joints (up to 8 nm) and is thinner at the sticking-out corners (down to 3 nm).

3.2. Photoelectrochemical Characterizations. The effect of the La^{3+} surface modification on electronic conductivity of photoanodes can be investigated by the photoelectrochemical measurement of the electron transfer resistance.[21] For this measurement, all the electrodes (control and modified films) were subject to the linear sweep voltammetry (LSV) measurement under the UV illumination with various intensities. Panels a and b in Figure 4 show the typical LSV

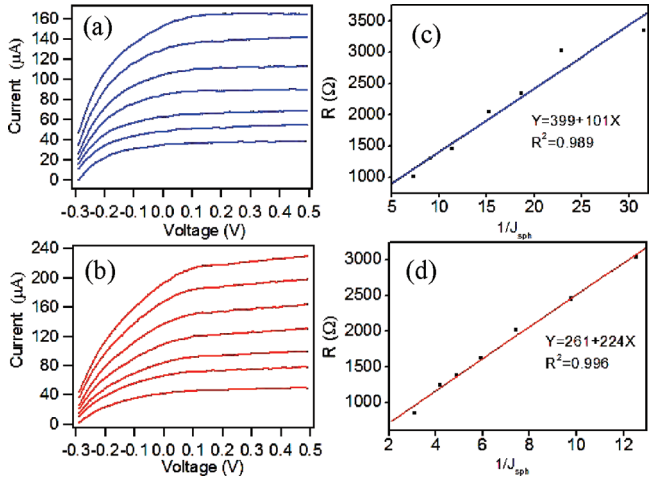

Figure 4. Voltammograms of the (a) control film and (b) M8 modified film under various light intensities in 0.1 M $NaNO_3$ solution. Scan rate was 5 mV/s. Light intensity for curves (from top to bottom) were 9.8, 9.2, 8.2, 7.2, 6.2, 5.2, and 4.2 mW/cm^2, respectively. Relationship between calculated resistances and inversed saturation photocurrents of the (c) control film and (d) modified film. Data were derived from a and b.

voltammograms for the electrodes. It was observed that each voltammogram ($J_{ph} - E$) under a given light intensity consists of two stages (see Figure 4a, b). In a potential bias range from −0.3 to 0.0 V, the photocurrent response increased monotonically with the applied potential bias. Under such conditions, the system behaved like a pure resistor. Therefore, Ohm's law was used to calculate the total electronic resistance, i.e., $R = (E_2 - E_1)/(I_2 - I_1) = \Delta E/\Delta I$. In contrast, when potential bias was greater than ca. 0.0 V, the photocurrent levelled off, reaching a saturation photocurrent (J_{sph}). Using computer linear regression fitting, the obtained R values were plotted against the reciprocal of the saturation current (i.e. $1/J_{sph}$), giving an excellent linear regression equation as eq 1.[21]

$$R = k/J_{sph} + R_0 = R_I + R_0 \quad (1)$$

R consists of two parts: a variable resistance (R_I) and an intrinsic resistance (R_0) (Eqn.1). R_I depends on experimental conditions that affect the interfacial reaction such as light intensity and reaction media. It is therefore reversely proportional to I_{sph}. The intrinsic resistance R_0 corresponds to the sum of all Ohmic resistances, including TiO_2 crystal boundary resistances and the resistances at TiO_2/conducting substrate interface during electron transport.[21] Figure 4c and 4d show that the R_0 value for the control and modified films (M8) are 399 Ω and 261 Ω, respectively. This indicates that the photoelectron transfer resistance is considerably reduced by the La^{3+} modification and confirms the improved electronic conductivity of the film.

dx.doi.org/10.1021/am2015553 | ACS Appl. Mater. Interfaces 2012, 4, 1289−1294

Similarly, a series of R_0 values were obtained for the modified samples (see Table 1). The effect of La^{3+} on the conductivity of the TiO_2 lies in the passivation effect. It could form a blocking layer for electron transfer due to the higher energy bandgap of the La_2O_3 ($E_g \approx 5.5$ eV). Table 1 show that the R_0 value increases slightly with the first coating times due to the electron blocking effect, then decreased gradually down to 261 Ω for M8 because of the improved electric conductivity before a sharp increase for M10. Overall, M8 is the optimum sample with the minimum resistance among the modified samples.

3.3. Dye Adsorption. The La^{3+} surface modification changes chemical composition of the photoanode surface and could alter the surface area of the photoanodes and therefore affect the dye adsorption amount and strength. The effect of the surface modification on the dye adsorption was therefore investigated. The surface areas of the photoanodes were firstly quantified by the BET method and are displayed in Table 1. The surface area decreased gradually with the increase of coating times from 61.53 to 53.20 m^2/g. This can be explained by the pore-filling effect from the surface modification process.

The dye adsorption amounts of the control and modified films were measured using the conventional NaOH ethanolic solution dye desorption method (see Table 1). The dye loading measurement was conducted by desorbing the adsorbed dye from the prepared films into the NaOH ethanolic solution and then measuring the absorbance of the resultant dye solution.[22] During the experiment, interestingly, we found that the dye anchored on the modified films is hard to achieve fully desorption in 4 h, whereas the desorption process could be finished in 2 h for the control films. This significant difference in the desorption time can be explained by the strong interaction between the dye molecules and the lanthanum, i.e., the formation of coordination complex bonding between the Lewis electrons of the functional groups of dye molecules and of f orbital of the lanthanum.[13]

Corresponding reductions of the dye loading amount on the film were expected as the film surface area decrease. However, Table 1 shows the modified films (M1−M10) had only a slightly decrease in dye loading amount compared with the control photoanodes. In particular, the calculated dye loading amounts for the control film and modified film were 1.67×10^{-7} mol/cm^2 and 1.64×10^{-7} mol/cm^2, respectively. This represents a decrease of 1.8%, which is in strong contrast with the decrease in surface area of 9%. The preservation of the dye loading amount suggests that the strong co-ordination complex bonding compensates the loss of the surface area. And this small decrease in dye loading amount is not likely to influence the photovoltaic performance of the DSSC.

3.4. DSSC Performance Evaluation. The DSSCs of the control and the La^{3+}-modified photoanodes were tested under 100 mW cm^{-2} illumination (AM 1.5G). The photocurrent as a function of voltage for the DSSCs was shown in Figure 5 and the corresponding photovoltaic characteristics derived from the $J-V$ curves were listed in Table 2. In comparison with the control film, the V_{oc} were improved for all modified photoanodes. Among them, the sample M10 showed the most significant 4.6% improvement in V_{oc} from 684 mV to 716 mV, While the sample M8 showed the largest improvement in J_{sc} from 14.93 to 22.21 mA/cm^2. Hence, the solar energy conversion efficiency for the M8 was increased to 9.67%, which is a significant increase of 41.3% in comparison with that of the control film. The DSSCs performance in Table 2 suggested that the sample

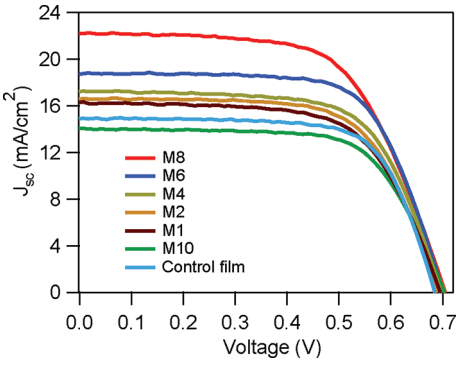

Figure 5. Dependence of the DSSC performance on the coating times of the organic lanthanum solution.

Table 2. DSSC Performance of the Control and Modified Films

electrodes	J_{sc} (mA cm^{-2})	V_{oc} (mV)	FF (%)	η (%)
control film	14.9	684	67	6.84
modified film (M1)	16.2	692	67	7.51
modified film (M2)	16.6	692	66	7.59
modified film (M4)	17.2	701	66	8.07
modified film (M6)	17.8	698	68	8.51
modified film (M8)	22.2	704	62	9.67
modified film (M10)	14.1	716	66	6.64

M8 was the optimum photoanode for the DSSCs in terms of the photo-to-electricity conversion efficiency.

It is noticeable that the photocurrent achieved for M8 in this work is relatively high among the DSSCs using N719 dye. This is not unexpected considering the theoretical photocurrent density for the N719 dye can be as high as 25 mA cm^{-2}[23] and similar photocurrent densities have been achieved in the literature, for examples, 21.9 mA cm^{-2} was obtained by Muduli et al.[24] The reasons for this are explored as follows.

The performance of the DSSCs is commonly influenced by dye loading and electron transport efficiency.[25] The dramatic improvements of the DSSCs performance as shown in Table 2 were apparently resulted from the La^{3+} modification. First, despite the decreased surface area, the dye loading of the modified film was well-maintained because of the stronger interactions between the dye molecule and lanthanum. Second, the electron transfer resistance of the photoanodes was significantly reduced by the La^{3+} modification, which was confirmed by the photoelectrochemical measurement. The latter is beneficial to the reduction of electron recombination. The reduction of the electron recombination can be further confirmed by the dark current and open-circuit voltage decay (OCVD) measurement.

Dark currents were measured in the dark using LSV techniques and shown in Figure 6. The dark currents in DSSCs are not directly related to the back electron transfer process under illumination, because the electrolyte concentration in the films and the potential distribution across the nanoporous electrode in the dark are different than those under illumination. However, it is well-established that the dark current magnitude and onset reflect the bare FTO area that is closely related to the back electron transfer, i.e., electron recombination at the FTO/electrolyte interface. Therefore, the decrease of the dark current and the increase of dark current onset have been commonly used to qualitatively describe the inhibition of the back electron

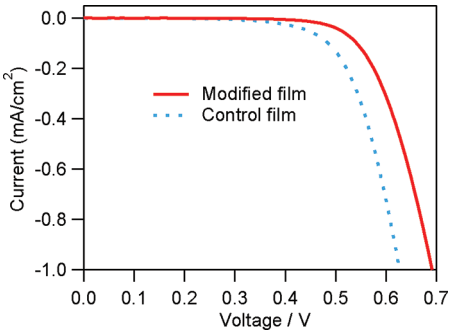

Figure 6. Voltammograms of the DSSCs with the control and M8 modified films in the dark.

transfer.[26] The voltammograms of the DSSCs with the control and the M8 modified film in the dark are shown in Figure 6. The results showed that the onset of dark current for DSSC with the control film occurred at a low potential bias ca. +0.4 V, whereas for the modified film, the onset potential shifted to 0.5 V. Besides, under the same applied bias over 0.45 V, the cells with the control film showed a higher dark current compared with that of the modified film. The lower dark current of the modified photoanodes indicates the back electron transfer process was suppressed.

Furthermore, the electron recombination in DSSC can be characterized by the OCVD technique.[27] This measurement was conducted when a steady-state open-circuit voltage (V_{oc}) of the DSSC was obtained under the solar light illumination and the decay of V_{oc} was monitored after the stop of the illumination. It is well-established that V_{oc} is highly dependent on the quasi-Fermi level, i.e., the electron density at the CB of TiO_2. Therefore, the decay of V_{oc} can be used to reflect the regression of electron density at the CB of TiO_2.[28] Figure 7 shows that the

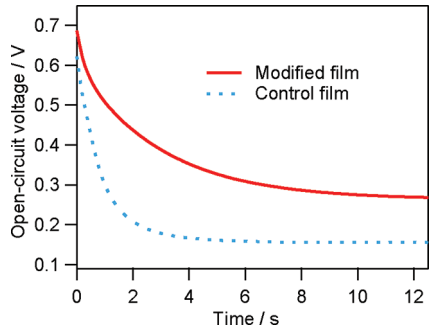

Figure 7. Open-circuit voltage decay curves of the DSSCs with the control and M8 modified films.

decay rate of V_{oc} with the modified film was much slower than that with the control film. This indicates a restrained regression of electron density at the CB of the modified TiO_2, and suggests that the recombination rate at the modified film was considerably reduced and leads to more photoelectrons survive through the electron transport process and stronger photocurrent. In addition, the alleviated electron recombination could increase the electron density at the conduction band, which raised the Fermi level and V_{oc}.

4. CONCLUSIONS

La_2O_3-modified TiO_2 nanoporous photoanodes were fabricated for dye-sensitized solar cells by a dip-coating method using an organic lanthanum solution. The formation of coordination bonding between the lanthanide ions and dye molecules enhances the dye adsorption. Moreover, photoelectrochemical characterization results demonstrate that the modified photoanodes possess lower electron transfer resistance than the original TiO_2 photoanodes, which alleviates the electron recombination rate. The XRD and XPS analyses suggest the presence of La^{3+} in the modified photoanodes. Consequently, the overall energy conversion efficiency of the La_2O_3 modified DSSCs was dramatically boosted to 9.67% in comparison with 6.84% of the original DSSCs.

AUTHOR INFORMATION

Corresponding Author

*Tel: (61-7) 5552 8155. Fax: (61-7) 5552 8067. E-mail: s.zhang@griffith.edu.au.

Notes

The authors declare no competing financial interest.

ACKNOWLEDGMENTS

The authors acknowledge the financial support of the ARC discovery grants from Australian Research Council.

REFERENCES

(1) O'Regan, B.; Graetzel, M. *Nature (London)* **1991**, *353*, 737.
(2) Bwana, N. *Nano Research* **2008**, *1*, 483.
(3) Green, M. A.; Emery, K.; Hishikawa, Y.; Warta, W. *Prog. Photovolt.: Res. Appl.s* **2011**, *19*, 84.
(4) Gratzel, M. *Prog. Photovoltaics* **2000**, *8*, 171.
(5) Haque, S. A.; Tachibana, Y.; Klug, D. R.; Durrant, J. R. *J. Phys. Chem. B* **1998**, *102*, 1745.
(6) Wu, X.; Wang, L.; Luo, F.; Ma, B.; Zhan, C.; Qiu, Y. *J. Phys. Chem. C* **2007**, *111*, 8075.
(7) Diamant, Y.; Chappel, S.; Chen, S. G.; Melamed, O.; Zaban, A. *Coord. Chem. Rev.* **2004**, *248*, 1271.
(8) Taguchi, T.; Zhang, X.-t.; Sutanto, I.; Tokuhiro, K.-i.; Rao, T. N.; Watanabe, H.; Nakamori, T.; Uragami, M.; Fujishima, A. *Chem. Commun. (Cambridge, U. K.)* **2003**, 2480.
(9) Palomares, E.; Clifford, J. N.; Haque, S. A.; Lutz, T.; Durrant, J. R. *J. Am. Chem. Soc.* **2003**, *125*, 475.
(10) Menzies, D. B.; Bourgeois, L.; Cheng, Y. B.; Simon, G. P.; Brack, N.; Spiccia, L. *Surf. Coat. Technol.* **2005**, *198*, 118.
(11) Zaban, A.; Chen, S. G.; Chappel, S.; Gregg, B. A. *Chem. Commun. (Cambridge)* **2000**, 2231.
(12) Kay, A.; Graetzel, M. *Chem. Mater.* **2002**, *14*, 2930.
(13) Zhang, Y.; Xu, H.; Xu, Y.; Zhang, H.; Wang, Y. *J. Photochem. Photobiol., A* **2005**, *170*, 279.
(14) Zhang, S.; Zheng, Z.; Wang, J.; Chen, J. *Chemosphere* **2006**, *65*, 2282.
(15) Yu, H.; Zhang, S.; Zhao, H.; Xue, B.; Liu, P.; Will, G. *J. Phys. Chem. C* **2009**, *113*, 16277.
(16) Yu, J.-G.; Yu, H.-G.; Cheng, B.; Zhao, X.-J.; Yu, J. C.; Ho, W.-K. *J. Phys. Chem. B* **2003**, *107*, 13871.
(17) Vadivel Murugan, A.; Navale, S. C.; Ravi, V. *Mater. Lett.* **2006**, *60*, 848.
(18) Reddy, B. M.; Sreekanth, P. M.; Reddy, E. P.; Yamada, Y.; Xu, Q.; Sakurai, H.; Kobayashi, T. *J. Phys. Chem. B* **2002**, *106*, 5695.
(19) Liu, M.; Piao, L.; Zhao, L.; Ju, S.; Yan, Z.; He, T.; Zhou, C.; Wang, W. *Chem. Commun.* **2010**, *46*, 1664.
(20) Wang, Z. L.; Colliex, C.; Paul-Boncour, V.; Percheron-Guegan, A.; Achard, J. C.; Barrault, J. *J. Catal* **1987**, *105*, 120.
(21) Jiang, D.; Zhao, H.; Zhang, S.; John, R. *J. Phys. Chem. B* **2003**, *107*, 12774.
(22) Kakiuchi, K.; Hosono, E.; Fujihara, S. *J Photochem. Photobiol., A* **2006**, *179*, 81.
(23) Snaith, H. J. *Adv. Funct. Mater.* **2010**, *20*, 13.

(24) Muduli, S.; Lee, W.; Dhas, V.; Mujawar, S.; Dubey, M.; Vijayamohanan, K.; Han, S.-H.; Ogale, S. *ACS Appl. Mater. Interface* **2009**, *1*, 2030.
(25) Graetzel, M. *C. R. Chim.* **2006**, *9*, 578.
(26) Green, A. N. M.; Palomares, E.; Haque, S. A.; Kroon, J. M.; Durrant, J. R. *J. Phys. Chem. B* **2005**, *109*, 12525.
(27) Zaban, A.; Greenshtein, M.; Bisquert, J. *ChemPhysChem* **2003**, *4*, 859.
(28) Oekermann, T.; Zhang, D.; Yoshida, T.; Minoura, H. *J. Phys. Chem. B* **2004**, *108*, 2227.